Acoust. Sci. & Tech. **30**, 2 (2009)

TECHNICAL REPORT

Shear modulus reconstruction by strain tensor measurement using lateral modulation

Chikayoshi Sumi*

Department of Information and Communication Sciences, Faculty of Science and Technology, Sophia University, 7–1, Kioicho, Chiyoda-ku, Tokyo, 102–8554 Japan

(*Received 4 October 2007, Accepted for publication 6 August 2008*)

Abstract: Two-dimensional (2D) shear modulus reconstructions are performed on an agar phantom using our previously developed ultrasound lateral Gaussian envelope cosine modulation method (LGECMM) together with multidimensional displacement vector measurement methods, i.e., the multidimensional cross-spectrum phase gradient method (MCSPGM), the multidimensional autocorrelation method (MAM) and the multidimensional Doppler method (MDM). The accuracies of the obtained 2D reconstructions are compared with each other in addition to those of 1D reconstructions obtained from the respective ratios of lateral and axial strains.

Keywords: Shear modulus reconstruction, Ultrasound, Lateral modulation, Displacement vector measurement, Strain tensor measurement, Phantom experiment

PACS number: 43.80.Qf, 43.80.Vj, 43.35.Yb, 43.60.Lq [doi:10.1250/ast.30.124]

1. INTRODUCTION

We previously reported three methods of measuring a multidimensional displacement vector using an ultrasound (US) signal phase, i.e., the multidimensional autocorrelation method (MAM) [1,2], the multidimensional Doppler method (MDM) [1,2] and the multidimensional cross-spectrum phase gradient method (MCSPGM) [3,4]. These methods can be applied to the measurement of tissue strain tensors for shear modulus reconstruction (e.g., breast and liver) [5–7], blood flow vectors, sonar data and other target motions. Briefly, in MCSPGM [3,4], a local displacement vector is estimated using the local echo phase characteristics, i.e., from the gradient of the phase of the local cross-spectrum evaluated from the local region echo data. In contrast, the other two methods use an instantaneous US phase [1,2]. However, all the methods enable *simultaneous* axial and lateral displacement measurements. The measurement accuracies and computational loads of the methods are compared in [2]. Another displacement vector measurement method [8] and various axial displacement measurement methods (see references in [2]) have also been reported.

Generally, when using such displacement vector measurement methods, the measurement accuracy of lateral displacement is lower than that of axial displacement [1–4]. However, even if the target predominantly moves or deforms in the lateral direction, the simultaneous measurements result in the accurate measurement of axial displacement without lateral modulation [9]. However, a high vector measurement accuracy is achieved by combining such a vector measurement method with our previously developed lateral Gaussian envelope cosine modulation method (LGECMM) [1,2]. In particular, these methods improve the measurement accuracy of lateral and elevational displacements, although such a lateral modulation method also improves the measurement accuracy of axial displacement.

In the field of blood flow measurement, such a lateral modulation approach [10] using a Fraunhofer approximation [11] has already been applied by other groups [12,13]. In the field of strain measurement, such an approach has also been applied [14,15]. However, for our tissue shear modulus reconstruction [6,7], to realize comparably high measurement accuracies for axial and lateral displacements, lateral modulation frequency is significantly increased [1,2,14] compared with that observed in the reported application to blood flow [12,13] and tissue strain measurement [15]. Deeply situated tissues must also be considered (e.g., liver). Thus, suitable focusing is also performed, i.e., spherical focusing [1,2,14]. Although the

*e-mail: c-sumi@sophia.ac.jp

modulation methods described in [12,13,15] yield band-unlimited, modulated spectra using infinite-length apodization functions (e.g., ringing expressed by sinc functions), our developed LGECMM realizes band-limited, modulated spectra using a finite-length apodization function. LGECMM causes no aliasing.

Thus far, various applications of axial strain measurements have been reported using axial [16] and multidimensional [17] displacement measurement methods, but without lateral modulation (e.g., diagnosis of cancers of human *in vivo* breast [16,17]). In [17], we made manual strain measurement possible by developing multidimensional rf-echo phase matching [3,4]. However, reports on shear modulus reconstruction using measured strain tensor distributions are limited except for our reports (e.g., [18–21]) and the reconstruction using a measured axial displacement distribution (e.g., [22]). In [18,19], we reported two-dimensional (2D) shear modulus reconstruction using regularized strain tensor measurement [20] as well as regularized 2D shear modulus reconstruction [20,21] using raw strain tensor measurement. These multidimensional reconstructions have only been stably achieved on agar phantoms using our developed method of *spatially variant regularization*, although on human *in vivo* tissues (e.g., breasts [6,18,23] and livers [6,20,21]) only 1D reconstructions using axial strain have been achieved (i.e., using the axial strain ratio [3,9,17] and regularized implicit integration [6,23]). However, the 2D and 1D reconstructions with only regularization yield no accurate reconstruction value. Moreover, 1D reconstruction using the axial strain is ineffective when the target deforms predominantly in the lateral direction [9].

In this report, we show 2D shear modulus reconstruction results obtained on an agar phantom in such a lateral deformation case by applying LGECMM together with MCSPGM [24], MAM and MDM (Sect. 2). That is, the target agar phantom was predominantly compressed in the lateral direction, the displacement of which cannot be accurately measured by conventional beamforming. In Sect. 3, we provide a discussion and conclusions.

2. PHANTOM EXPERIMENTS ON AGAR PHANTOM

We have generated a target agar phantom [33 (axial) × 70 (lateral) × 40 (elavational) mm] having a central circular cylindrical inclusion (diameter, 10 mm; depth, 19 mm) with a shear modulus different from that of the surrounding region. Elasticity was controlled by adjusting the agar concentration. The agar concentrations in the cylindrical inclusion and surrounding regions were 7.0 and 3.0%, respectively. To control US attenuation, graphite powder (concentration, 3.0%) was also added. The resultant phantom had shear moduli of 3.20 and $0.86 \times 10^6\,\mathrm{N/m^2}$ in the inclusion and surrounding regions, respectively. Thus, the relative shear modulus was 3.7. The phantom was manually compressed by 1.0 mm in the lateral direction. The contact surfaces of the transducer and phantom were separated by immersing them in water in a tank; a sponge was placed under the phantom to allow the phantom to elongate in the axial direction by lateral compression from the right-hand side using a large plate (as in Case 1 in [9]). The left surface was fixed to a wall.

The US transducer (LNR5539, Aloka Co., Ltd., Tokyo, Japan) was of the conventional linear array type with a nominal frequency of 7.5 MHz. RF-echo data were digitized with a 12-bit resolution at a sampling rate of 30 MHz. RF-echo data had sampling intervals of 0.0255 and 0.1000 mm in the axial and lateral directions, respectively (US speed was assumed to be 1,530 m/s). Because we have no real-time beamformer, we used a classical synthetic aperture (specifically, a monostatic one). A rectangular region of interest (ROI) of 11.5 (axial) × 11.8 (lateral) mm was centered on the inclusion (depths, 13.4 to 24.9 mm).

2.1. Modulations

Figure 1 shows the 2D spectra obtained for the ROI by (a) conventional beamforming (i.e., nonmodulation) and (b)–(i) LGECMM at modulation frequencies of

(b) 3.75 MHz by transmitting and receiving spherical focusings; and transmitting and receiving apodizations,

(c) 1.875 (3.75/2) and (d) 3.75 MHz by only receiving spherical focusing; and only receiving apodization,

(e) 7.5 MHz by transmitting and receiving spherical focusings; and transmitting and receiving apodizations,

(f) 3.75 MHz by transmitting axicon focusing and receiving spherical focusing; and only receiving apodization,

(g) 3.75 MHz realized by (f) plus transmitting apodization,

(h) 3.75 MHz by transmitting and receiving axicon focusings; and transmitting and receiving apodizations and

(i) 3.75 MHz by only receiving axicon focusing; and only receiving apodization.

In addition, Figs. 2(a) and 2(b) respectively show B-mode images (square detection) obtained from the spectra in Figs. 1(a) (conventional beamforming) and 1(b) (3.75 MHz modulation). As shown, the lateral speckle size in Fig. 2(b) is smaller than that in Fig. 2(a).

As confirmed from the spectra in Figs. 1(b)–1(i) and 2(a) and 2(b), we succeeded in lateral modulation using LGECMM. That is, nonringing spectra with the modulation frequencies (7.5, 3.75, 1.875 MHz) could be obtained. The modulated echo data in Figs. 1(b) and 1(c) were obtained using the same effective aperture size. That is, focusing and apodization in both the transmission and reception [Fig. 1(b)] enabled us to achieve the same modulation

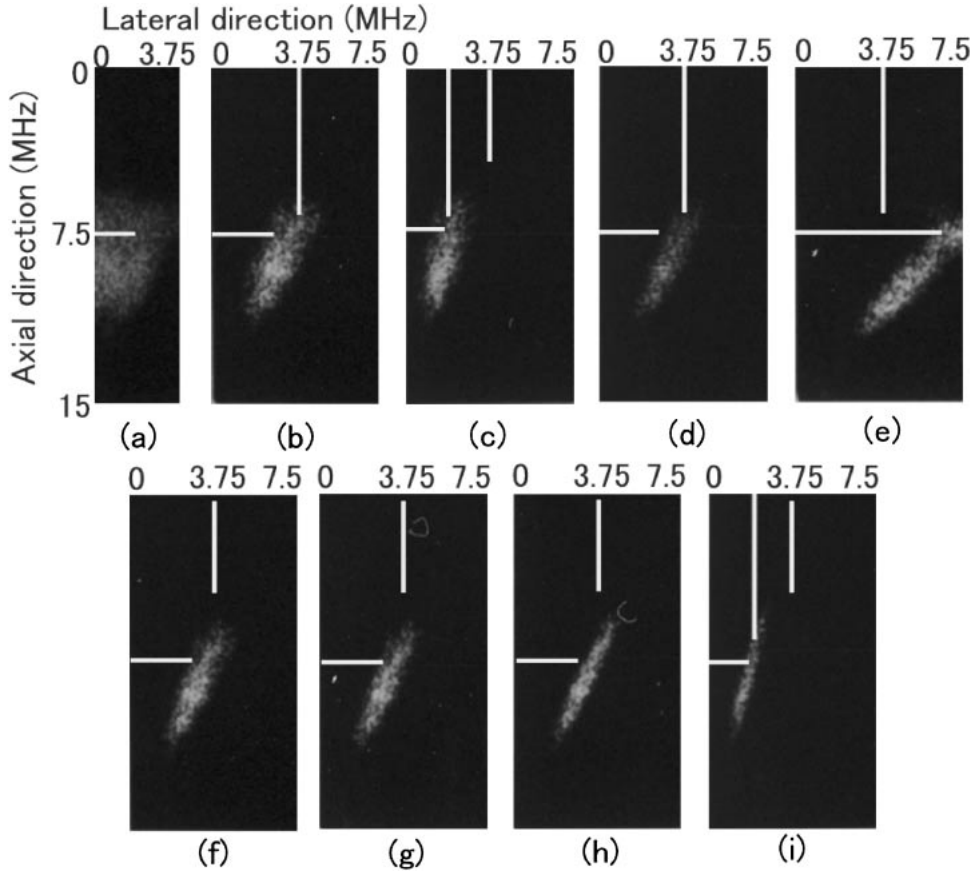

Fig. 1 Two-dimensional (2D) spectra obtained by (a) conventional beamforming (i.e., nonmodulation) and (b)–(i) lateral modulation (LGECMM) at modulation frequencies of (b) 3.75 MHz by transmitting and receiving spherical focusings and transmitting and receiving apodizations, (c) 1.875 (3.75/2) and (d) 3.75 MHz by only receiving spherical focusing and only receiving apodization, (e) 7.5 MHz by transmitting and receiving spherical focusings and transmitting and receiving apodizations, (f) 3.75 MHz by transmitting axicon focusing, receiving spherical focusing and only receiving apodization, (g) 3.75 MHz realized by (f) plus transmitting apodization, (h) 3.75 MHz by transmitting and receiving axicon focusings and transmitting and receiving apodizations, and (i) 3.75 MHz by only receiving axicon focusing and only receiving apodization. The nominal ultrasound frequency, 7.5 MHz.

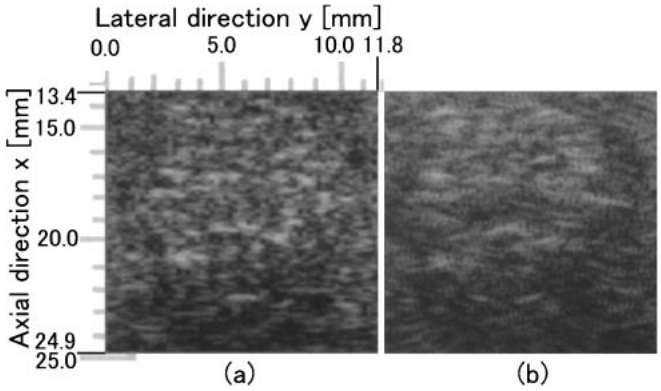

Fig. 2 B-mode images for ROI obtained by square detection for (a) conventional beam-forming [i.e., no lateral modulation of spectra in Fig. 1(a)] and (b) 3.75 MHz lateral modulation of spectra in Fig. 1(b).

frequency (3.75 MHz) using a smaller effective aperture size than that used for only reception [Fig. 1(d)]. Also note that the bandwidth in Fig. 1(b) is wider than that in Fig. 1(d). The use of the transducer also enabled us to increase the lateral modulation frequency up to almost 7.5 MHz, i.e., Fig. 1(e) (however, exactly less than 7.5 MHz). However, echo signal-to-noise ratio (SNR) significantly decreased, as shown by the darker spectra in Fig. 1(e) than in Fig. 1(b). This was also confirmed by simulations and will be reported in detail elsewhere. Also note that, as confirmed by Figs. 1(b) and 1(e), the increase in modulation frequency decreased the bandwidth, similarly to the cases when only receiving modulations were performed [Figs. 1(c) and 1(d)]. This has already been confirmed by simulations in [2].

The modulation shown in Fig. 1(f) can be realized for an ROI in real time, i.e., by transmitting two plane waves successively or simultaneously with the same steering angle as those in the case shown in Fig. 1(b). The bandwidth in Fig. 1(f) became less than that in Fig. 1(b). However, this is not because no apodization is performed in the transmission. This can be confirmed from Fig. 1(g), i.e., the case shown in Fig. 1(f) plus transmitting apodization.

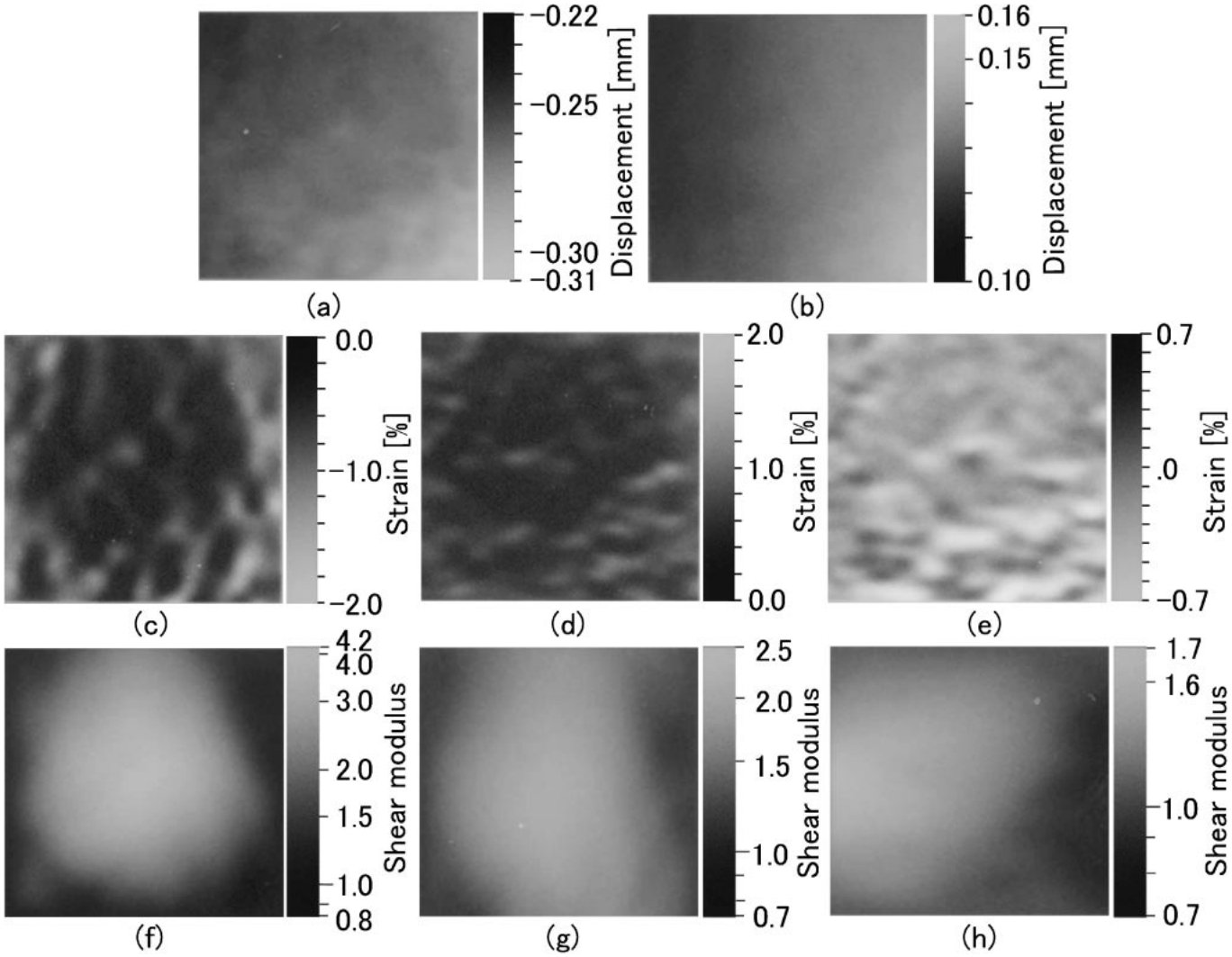

Fig. 3 Results obtained using MCSPGM: measured (a) lateral displacement dy and (b) axial displacement dx, (c) lateral strain ε_{yy}, (d) axial strain ε_{xx} and (e) shear strain ε_{xy}; (f) 2D shear modulus reconstruction, and 1D shear modulus reconstructions using ratios of (g) lateral and (h) axial strain.

That is, when performing axicon focusing, Gaussian apodization is not effective for increasing the bandwidth. The ineffectiveness can also be confirmed from the differences between the bandwidths obtained by spherical and axicon focusings by comparing Figs. 1(b) and 1(h) and Figs. 1(c) and 1(i).

2.2. 2D Shear Modulus Reconstruction by Measurement of 2D Displacement Vector/2D Strain Tensor

Next, 2D shear modulus reconstructions [5,6] were performed using laterally modulated echo data. For the measurement of the 2D displacement vector, MCSPGM [3,4], MAM [1,2] and MDM [1,2] were used. For 2D reconstruction, the method using a typical Poisson's ratio (0.5) was used under a 2D stress condition. Because the phantom was predominantly deformed in the lateral direction, the reference region was set on the right borderline of the ROI. For comparison, nonmodulated echo data were also used together with MCSPGM. The measured displacements obtained using the methods are shown in Figs. 3–6, i.e., (a) lateral displacement dy and (b) axial displacement dx. The local region used for phase matching [2–4] was 1.6×0.8 mm. The obtained 2D shear modulus reconstructions are also shown in (f) together with the lateral, axial and shear strains ε_{yy}, ε_{xx} and ε_{xy} in (c)–(e), respectively. The cutoff frequency of the differential filter used was $0.88\,\mathrm{mm}^{-1}$.

As confirmed in the strain images obtained from the modulated echo data (Figs. 3–5), the stiff inclusion could not be detected to be circular, although it was detected to be stably circular in the 2D shear modulus reconstructions, particularly when using MCSPGM and MAM [Figs. 3(f) and 4(f), respectively]. The phantom was not accurately deformed in the lateral direction. This was also confirmed from the displacement images (a) and (b). Table 1 shows the means and standard deviations (SDs) of the shear moduli evaluated in the central rectangular region

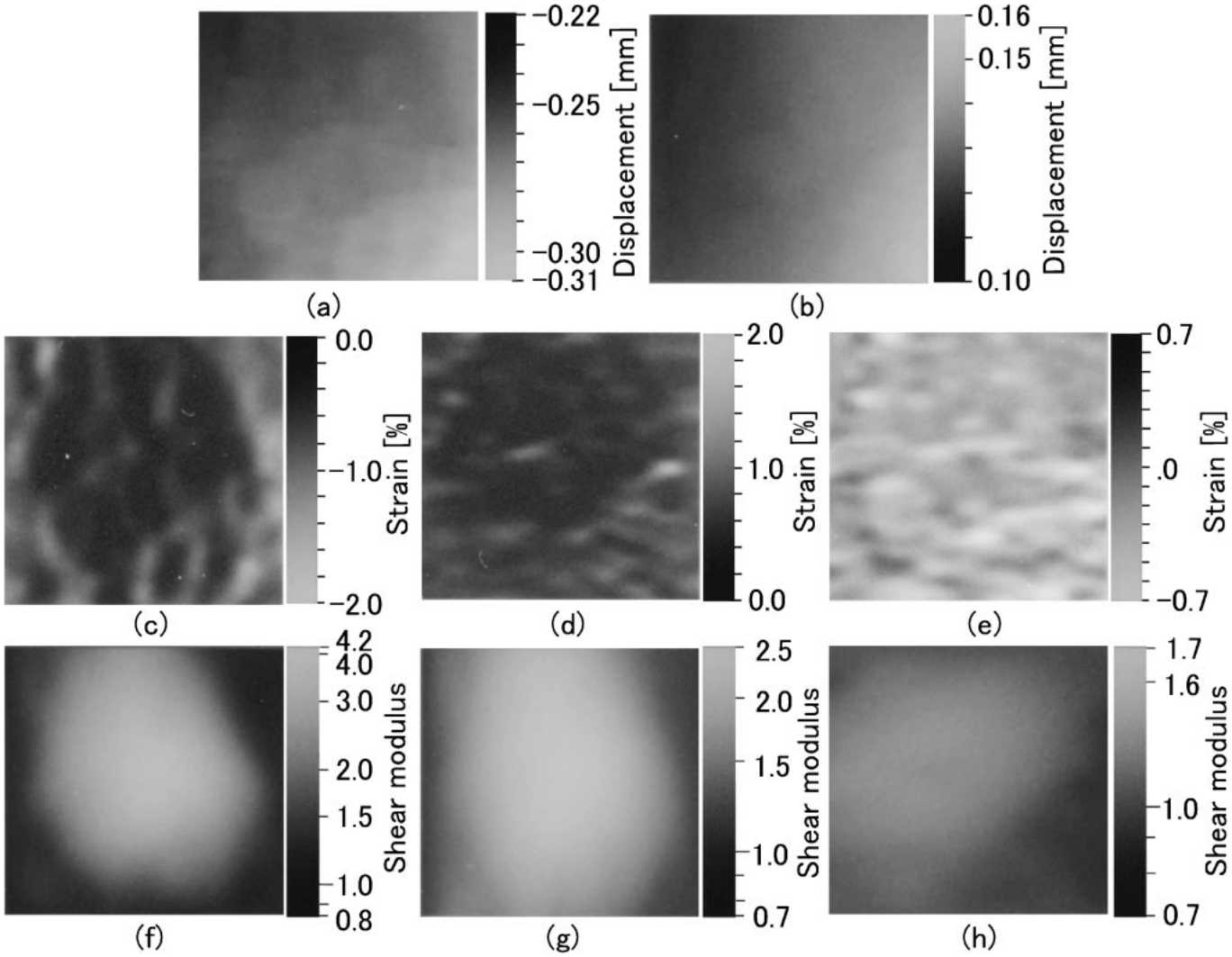

Fig. 4 As Fig. 3 using MAM.

(4.0 × 4.2 mm) in the inclusion. As shown, the relative shear modulus of the inclusion was accurately evaluated (means, 3.75 for MCSPGM and 3.77 for MAM). The result of MDM (Fig. 5) was unstable and inaccurate compared with those of MCSPGM and MAM (SD, 0.30 vs 0.28; mean, 3.34). The difference between the measurement accuracy of MDM and those of MCSPGM and MAM [2] results in a difference in reconstruction accuracy. According to the simulation results [2], we can conclude that the obtained modulated echo data has a high SNR.

Fortunately, in the nonmodulated case, the stiff region was also detected in the strain and shear modulus images [Figs. 6(c)–6(f)], although the shape was distorted and the reconstruction value was inaccurate (mean, 1.55) due to the low measurement accuracy of the lateral displacement dy [Fig. 6(a)]. The reason for the distortion can also be confirmed by comparing the principal lateral strain [Fig. 6(c)] with the reconstruction [Fig. 6(f)]. However, in most of the lateral deformation cases, it is difficult to detect even such a stiff region in the lateral strain image and shear modulus reconstruction.

In addition, two 1D reconstructions were also performed for all the echo data, i.e., from the lateral strain ratio and axial strain ratio. In the reconstruction using the axial strain ratio, the reference line was set at the upper borderline of the ROI. The results are shown in (g) and (h) in Figs. 3–6. Because the phantom was predominantly deformed in the lateral direction, particularly for the lateral modulation data, the lateral strain ratio might yield an equally useful shear modulus reconstruction as the axial strain ratio in the case where the target is predominantly deformed in the axial direction [3,23]. However, as mentioned above, because the phantom was not accurately deformed in the lateral direction, although the existence of the stiff region could be confirmed in the 1D reconstructions, the estimated shape of the inclusion was not circular. In addition, the estimated mean shear moduli were smaller than that obtained by simulations (3.1 vs 1.91 to 2.37), although originally the dynamic range of stiffness was estimated to be smaller than the original dynamic range

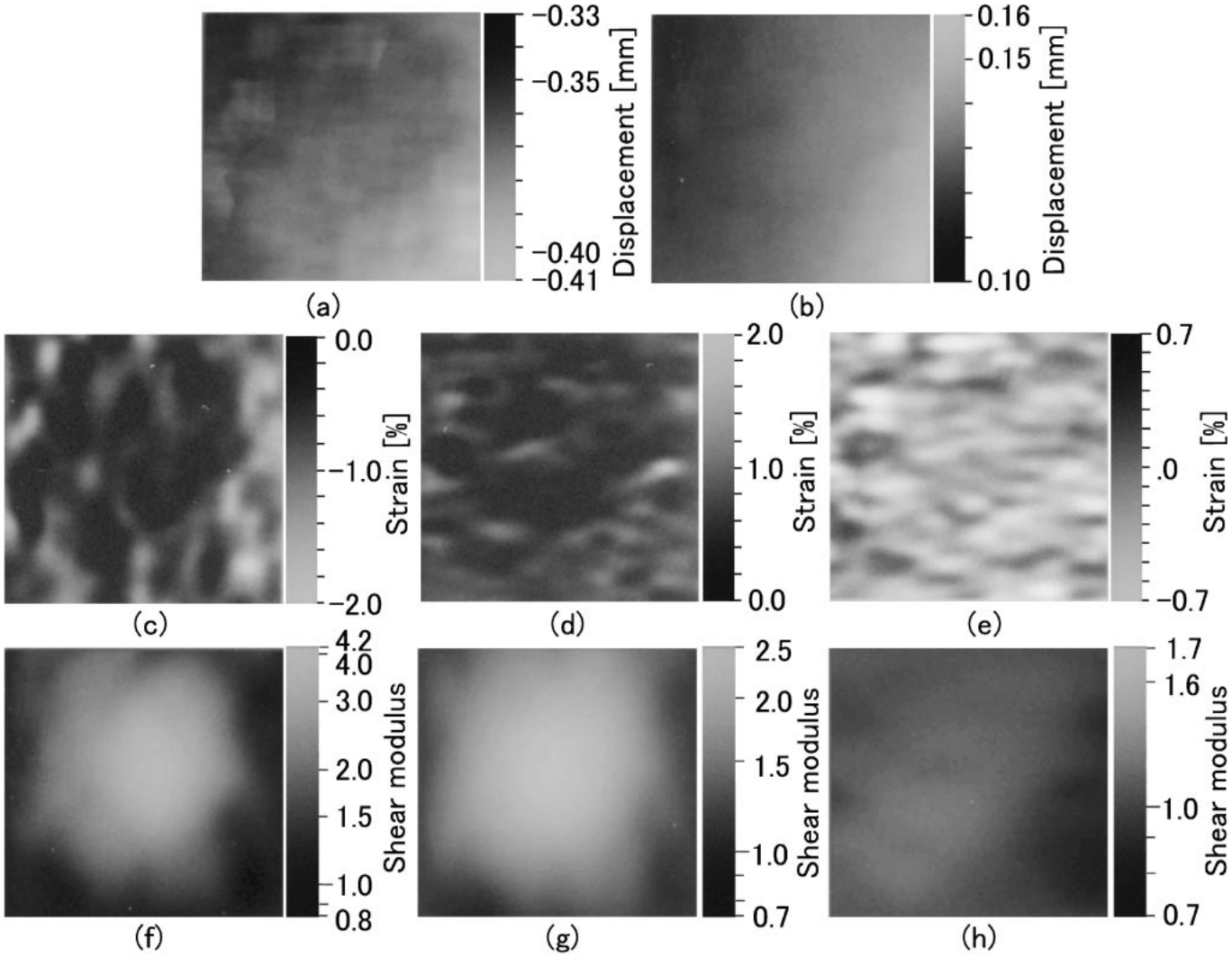

Fig. 5 As Fig. 3 using MDM.

(i.e., an artifact of the 1D reconstruction [6]). In addition, although the stiff region could be detected, the axial strain ratio yielded a much less useful reconstruction from the viewpoint of the accuracy of the reconstruction value than the lateral strain ratio, as shown in Case 1 in [9] (i.e., a lateral compression case). This can also be confirmed from Table 1 (means, 1.10 to 1.32). For the nonmodulated data, the reconstructed shapes of the stiff region were distorted [Figs. 6(g) and 6(h)] and the reconstruction values were inaccurate (means, 1.33 and 1.60).

3. DISCUSSIONS AND CONCLUSIONS

We succeeded in obtaining accurate shear modulus reconstruction values through actual strain tensor measurement. In our 2D reconstruction approach, only the assumption of 2D stress enabled accurate reconstruction [5,6]. In the phantom experiments, a difficult deformation case was dealt with. That is, in a conventional case, the principal strain cannot be accurately measured. Both the feasibility and the effectiveness of combining multidimensional displacement vector measurement methods and lateral modulation were confirmed by the experiment. This combination enables accurate, manual strain measurement and shear modulus reconstruction even for deep ROIs such as liver tissues, which are inaccessible from the body surface and are normally deformed by heart motion or pulsation. Only the attachment of a transducer will enable measurement and reconstruction by 3D processing. Note that lateral modulation is also useful for B-mode imaging.

In our approach, we have also improved LGECMM using parabolic functions or Hanning windows instead of Gaussian functions for the apodization function [25–30]. The new modulations enable a decrease in the effective aperture length (i.e., the required number of channels) and yield more accurate displacement vector measurements than LGECMM. Although the Fourier transforms of a parabolic function and a Hanning window result in ringing effects, the new modulations yield no ringing effects in the spectra. Thus, we no longer use a Fraunhofer approximation in lateral modulation [25–30]. In [25,28,31], we also

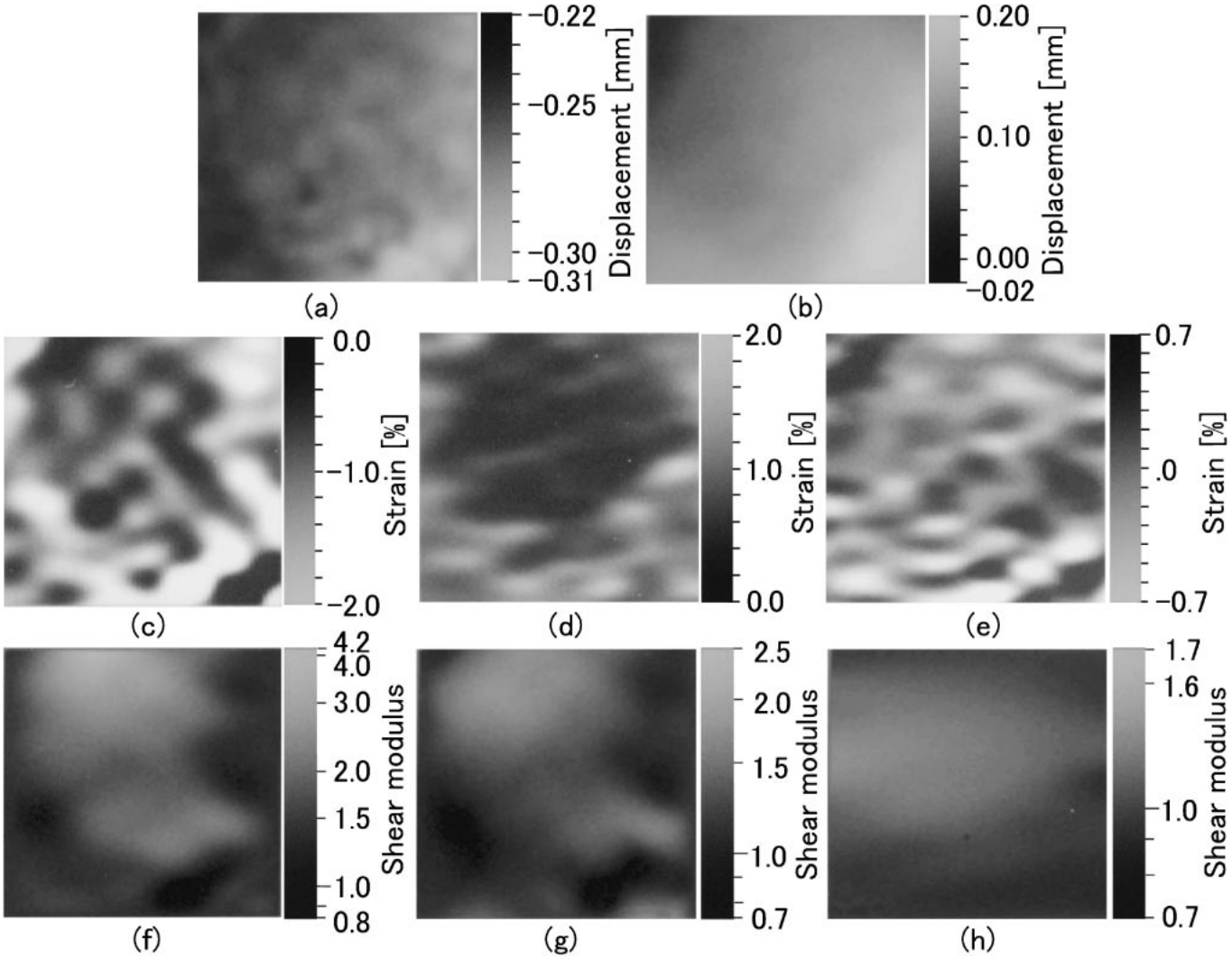

Fig. 6 As Fig. 3 using nonmodulated echo data together with MCSPGM.

Table 1 Means and standard deviations (SDs in parentheses) evaluated for two-dimensional (2D) shear modulus reconstruction in central rectangular region (4.0×4.2 mm) of stiff inclusion (relative shear modulus 3.7) obtained by MCSPGM, MAM and MDM for lateral modulated echo data and by MCSPGM for nonmodulated echo data. Values for 1D reconstructions obtained using axial and lateral strain ratios are shown together.

Disp./Recon.	2D	Lateral 1D	Axial 1D
MCSPGM	3.75 (0.28)	1.91 (0.11)	1.32 (0.10)
MAM	3.77 (0.28)	2.37 (0.10)	1.26 (0.05)
MDM	3.34 (0.30)	2.20 (0.12)	1.10 (0.03)
Nonmodulated	1.55 (0.18)	1.33 (0.16)	1.60 (0.11)

proposed to set the parameters of beamforming and the transducer to realize the required PSF on the basis of optimization theory. Such optimization will also be useful for B-mode imaging. The optimizations are outside the scope of this report.

REFERENCES

[1] C. Sumi, "Multidimensional displacement vector measurement methods utilizing instantaneous phase," *Proc. 27th Int. Conf. IEEE Eng. Med. Biol. Soc.*, CD-ROM (2005).

[2] C. Sumi, "Displacement vector measurement using instantaneous ultrasound signal phase—Multidimensional autocorrelation and Doppler methods" *IEEE Trans. Ultrason. Ferroelectr. Freq. Control*, **55**, 24–43 (2008).

[3] C. Sumi, A. Suzuki and K. Nakayama, "Phantom experiment on estimation of shear modulus distribution in soft tissue from ultrasonic measurement of displacement vector field," *IEICE Trans. Fundam.*, **E78-A**, 1655–1664 (1995).

[4] C. Sumi, "Fine elasticity imaging on utilizing the iterative rf-echo phase matching method," *IEEE Trans. Ultrason. Ferroelectr. Freq. Control*, **46**, 158–166 (1999).

[5] C. Sumi, A. Suzuki and K. Nakayama, "Estimation of shear modulus distribution in soft tissue from strain distribution," *IEEE Trans. Biomed. Eng.*, **42**, 193–202 (1995).

[6] C. Sumi, "Usefulness of ultrasonic strain measurement-based shear modulus reconstruction for diagnosis and thermal treatment," *IEEE Trans. Ultrason. Ferroelectr. Freq. Control*, **52**, 1670–1689 (2005).

[7] C. Sumi, "Reconstructions of shear modulus, Poisson's ratio and density using approximate mean normal stress as un-

known," *IEEE Trans. Ultrason. Ferroelectr. Freq. Control*, **53**, 2416–2434 (2006).

[8] J. A. Jensen, "A new estimator for vector velocity estimation," *IEEE Trans. Ultrason. Ferroelectr. Freq. Control*, **48**, 886–894 (2001).

[9] C. Sumi, "Ultrasonic axial strain measurement for lateral tissue deformation," *Ultrasound Med. Biol.*, **33**, 1830–1837 (2007).

[10] B. D. Steinberg, *Principles of Aperture and Array System Design* (Wiley, New York, 1976).

[11] J. W. Goodman, *Introduction to Fourier Optics*, 2nd ed. (McGraw-Hill, New York, 1996).

[12] J. A. Jensen, "A new method for estimation of velocity vectors," *IEEE Trans. Ultrason. Ferroelectr. Freq. Control*, **45**, 837–851 (1998).

[13] M. E. Anderson, "Multi-dimensional velocity estimation with ultrasound using spatial quadrature," *IEEE Trans. Ultrason. Ferroelectr. Freq. Control*, **45**, 852–861 (1998).

[14] C. Sumi, "Improvement of measurement accuracy of displacement vector by lateral modulation," *Proc. Autumn Meet. Acoust. Soc. Jpn.*, pp. 1353–1354 (2004) (in Japanese).

[15] H. Liebgott, J. Fromageau, J. E. Wilhjelm, D. Vray and P. Delachartre, "Beamforming scheme for 2D displacement estimation in ultrasound imaging," *EURASIP J. Appl. Signal Process.*, **8**, 1212–1220 (2005).

[16] B. S. Garra, E. I. Cespedes and J. Ophir, "Elastography of breast lesions: initial clinical results," *Radiology*, **202**, 79–86 (1997).

[17] C. Sumi, A. Suzuki, K. Nakayama and K. Kubota, "Estimation of stiffness distribution in soft tissue from displacement vector measurement," *Jpn. J. Med. Ultrason.*, **22** (Suppl. I), 44 (1995) (in Japanese).

[18] C. Sumi, "Our recent strain-measurement-based shear modulus reconstruction," *Proc. IEEE Int. Ultrason. Symp.*, pp. 1771–1776 (2005).

[19] C. Sumi, "Regularization for ultrasonic measurements of tissue displacement vector and strain tensor," *IEEE Trans. Ultrason. Ferroelectr. Freq. Control*, **55**, 787–799 (2008).

[20] C. Sumi, "Spatially variant regularization for tissue strain measurement and shear modulus reconstruction," *J. Med. Ultrason.*, **34**, 125–131 (2007).

[21] C. Sumi, "Regularization of tissue shear modulus reconstruction using strain variance," *IEEE Trans. Ultrason. Ferroelectr. Freq. Control*, **55**, 297–307 (2008).

[22] M. M. Doyley, S. Srinivasan and S. A. Pendergrass, "Comparative evaluation of strain-based and model-based modulus elastography," *Ultrasound Med. Biol.*, **31**, 787–802 (2005).

[23] C. Sumi and H. Matuzawa, "Shear modulus reconstruction using ultrasonically measured strain ratio," *J. Med. Ultrason.*, **34**, 171–188 (2007).

[24] C. Sumi, "Multidimensional tissue shear modulus reconstruction using ultrasonic lateral modulation and displacement vector measurement," *Proc. 13th Souhatu System Symposium* (*SICE*), pp. 139–142 (2007) (in Japanese).

[25] C. Sumi and T. Noro, "Lateral Gaussian envelope cosine modulation method (LGECMM) (4th report) — A breakaway from Fraunhofer approximation," *Proc. Autumn Meet. Acoust. Soc. Jpn.*, pp. 1035–1036 (2006) (in Japanese).

[26] C. Sumi, T. Noro, T. Ebisawa and T. Tooyama, "Increase in accuracies of MCSPGM, MAM and MDM," *5th Int. Conf. Ultrason. Meas. Imaging Tissue Elasticity*, p. 30 (2006).

[27] C. Sumi and A. Tanuma, "Lateral modulation and multidirectional synthetic aperture," *IEICE Tech. Rep.*, **US2007**, 13–18 (2007) (in Japanese).

[28] C. Sumi, "Beamforming for realizing designed point spread function" *IEEE 2007 Int. Ultrason. Symp.*, pp. 1557–1562 (2007).

[29] C. Sumi, T. Noro and A. Tanuma, "Effective lateral modulations with applications to shear modulus reconstruction using displacement vector measurement," *IEEE Trans. Ultrason. Ferroelectr. Freq. Control*, **55**, 2607–2625 (2008).

[30] C. Sumi and A. Tanuma, "Comparison of parabolic and Gaussian lateral cosine modulations in ultrasound imaging, displacement vector measurement, and elasticity measurement," *Jpn. J. Appl. Phys.*, **47**(5B), 4137–4144 (2008).

[31] C. Sumi, "A case of apodization function using singular value decomposition: Determination of beamforming parameters by optimization," *Acoust. Sci. & Tech.*, **29**, 185–187 (2008).